# CrystEngComm

Accepted Manuscript






ROYAL SOCIETY OF CHEMISTRY

www.rsc.org/crystengcomm

Cite this: DOI: 10.1039/c0xx00000x

www.rsc.org/xxxxxx

PAPER

# Formation of hierarchical structures of $Fe_2O_3$ by liquid-liquid interface technique

**Vibha Srivastava[1]* and Sanjeev Kumar[2]**

**Received (in XXX, XXX) Xth XXXXXXXXX 20XX, Accepted Xth XXXXXXXXX 20XX**

**DOI: 10.1039/b000000x**

We report formation of dendritic hierarchical structures α-$Fe_2O_3$ and nanostructures of $Fe_2O_3$ by simple liquid-liquid interface method. The morphology of thin films determined by high-resolution secondary electron microscope shows nanorods, nanosheet and dendritic $Fe_2O_3$. The identification of phases of iron oxide structures is carried out by using XRD and XPS studies. XRD and XPS measurements point to highly crystalline dendritic α- $Fe_2O_3$ phase and mixed phase of α and γ- $Fe_2O_3$ nanostructures. The magnetic measurement also suggests presence of mixed phase in the sample grown for 72 hours.

## Introduction

Microscale and nanoscale superlattices of inorganic materials have drawn attention due to their interesting electronic, optical, and magnetic properties,[1-4] and their potential application in photonics,[4] catalysis,[5] drug delivery,[6] etc. Self-assembly of dendritic crystals for synthesis of nanoscale superstructures has emerged as a cost effective and preferred route over the other methods[7]. The dendritic crystals, observed *in-situ* in supercooled water[8] on flat and curved interfaces consist of a main stem on which branches grow out[9]. The branches then act as main stems and the process repeats itself to finally generate hierarchical structures. Dendritic nanocrystals of a variety of materials have been synthesized using sonochemical method,[10] ultrasonic template assisted method,[11] organic agent reduction method,[12] chemical vapour deposition,[13] thermal evaporation,[14] etc. Cao et al.[15] have reported a hydrothermal method to produce dendritic crystals of hematite (α-$Fe_2O_3$). The method requires an aqueous solution of $K_3Fe(CN)_6$ to be autoclaved at 140°C for two days. Hematite finds applications in photocatalysis,[16] magnetic materials,[17] photochemical cells,[18] gas sensing,[19] lithium ion batteries,[20] etc. The n-type semiconducting α-$Fe_2O_3$ with a band gap of 2.1 eV at room temperature finds applications in photocatalysis,[16] photo-oxidation of water,[21] etc. Sun et al.[22] have recently used high temperature reduction of dendritic α-$Fe_2O_3$ using hydrogen gas to obtain Fe, γ-$Fe_2O_3$, and $Fe_3O_4$ while preserving the dendritic structure of the starting α-$Fe_2O_3$ material. γ-$Fe_2O_3$, which finds applications in memory devices, magnetic resonance imaging,[23] drug delivery and cell targeting,[6] etc., was produced in two steps. First, α-$Fe_2O_3$ was reduced for one hour at 350 °C in 10 ml/m hydrogen and 180 ml/m argon atmosphere to obtain $Fe_3O_4$. The later was then reduced for 2 hours in air at 140°C to obtain γ-$Fe_2O_3$.

Liquid-liquid interface technique has been employed in past to form thin film of metallic Ag[24], CuO and CuS[25]. We have used this technique to form dendritic structures of $Fe_2O_3$. In the present work, we report room temperature synthesis of dendritic α-$Fe_2O_3$ and γ-$Fe_2O_3$ by carrying out hydrolysis reaction on water-organic interface. The organic phase contains metal precursor and the aqueous phase contains a suitable agent for hydrolysis. The reaction occurs at the interface leading to the formation of dendritic structures there. To the best of our knowledge, this is the first report on synthesis of dendritic structures using liquid-liquid interface technique, and a room temperature route to formation of α-and γ-$Fe_2O_3$.

## Experimental section

The iron oxide nanoleaf or pine shaped dendritic structures are formed by employing iron cupferronate [$Fe(Cup)_3$] as metal source and NaOH as hydrolyzing agent. $Fe(Cup)_3$ is prepared by vigorously stirring aqueous solution of cupferron (Cup) with acidic solution of iron nitrate [$Fe(NO_3)_3$] at room temperature. The iron complex formed as brown precipitate is washed with dilute HCl to remove unreacted Cup and then re-crystallization is done in heptane. In order to produce an interface between two phases for reaction to occur, 25ml solution of 0.04M NaOH in milli-Q water was first taken in a 100ml beaker. The reddish brown coloured solution of 1mg $Fe(Cup)_3$ in 25 ml toluene (1 mM) was added to the beaker drop by drop. The reaction is followed at 6, 48, and 72 hours at room temperature. The free standing film formed at the interface between two liquid phases is carefully lifted and transferred on to a silicon substrate and dried for characterization. The morphology of the film is probed by Field Emission Scanning Electron Microscope (FESEM) Zeiss, Ultra 55, Germany. X-ray powder diffraction (PXRD) patterns are acquired at room temperature by employing Bruker D-8 advance Bragg-Brentano geometry with Cu Kα radiation (λ = 1.5418Å) using a scanning rate of 0.01° $S^{-1}$ in the 2θ range from 20−80°. X-ray photoelectron spectroscopy (SPECS, Germany) is carried out to identify chemical states of Fe in $Fe_2O_3$. The

magnetic properties were analyzed by SQUID (superconducting quantum interference device) magnetometer. The operating temperature range is 1.7K to 400K which can be changed in steps of 5K. A magnetic hysteresis loop measurement were performed by applying magnetic field normal to the substrate which can varied from 0 to 5T in steps of 0.5T.

## Results and discussion

The morphology of a free standing thin film is characterized by FESEM after transferring it onto a silicon substrate. In Figure 1, the left panel shows FESEM image of a film grown for 6 hours and the right panel shows a film grown for 48 hours. The film is characterized after six hours to understand the process of film formation. Figure 1a shows that the film has dendritic structures at nucleation stage itself, suggesting that the film formation commences at relatively higher supersaturation values than those required to form 2D islands. The average size of isolated $Fe_2O_3$ dendrites at this stage is around 1μm with a number density of ~$10^8 cm^{-2}$. The morphology of the film after 48 hours of growth is shown in Figure 1b. The observed feature appears like a tree fern of size 40μm, whose fronds consist of a midrib of size around 20μm with several veins or sub-branches arranged on either side. The sub-branches are of size around 1μm; the detailed structure of individual sub-branches could not be observed due to the limited resolution.

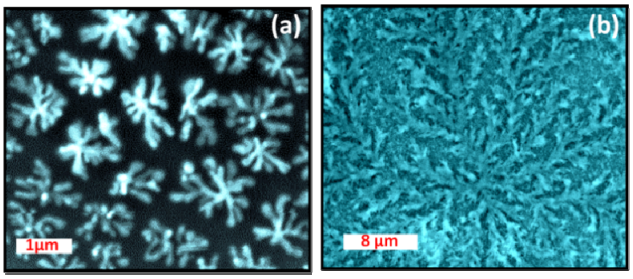


Figure 1 is an FESEM image of film formed after growth time (a) 6 hours, (b) 48 hours.

The growth time of the film was extended to 72 hours to decipher the final evolved state of the dendritic features observed at nucleation stage after six hours of growth. The FESEM images acquired at low as well as high resolution are shown in Figure 2. The low resolution FESEM image (Figure 2(a)) shows large fronds of length around 40 μm, with 500 nm wide central trunk and sub-branches of length around 4 μm on either side of the central trunk. Secondary features of size smaller than 2 μm are observed on top of the frond like features in some region of the image. High resolution imaging is carried out to provide intricate details of small features. Figure 2(b) shows that at high resolution majority of the structures appear like leaflets of a pine tree with 6-8 μm long central trunk and 1-2 μm long branches on either side. The ordered parallel branches of the dendritic structure are symmetrically distributed on both sides of the central trunk. Figure 2(c) shows further details of a branch: it is conical in shape, with around 500 nm wide base which narrows down to less than 100 nm at the pinnacle. The magnified view of these conical structures, shown in Figure 2(d), reveals that these consist of nanowires of high aspect ratio 80 (length and width of the wires are around 2 μm and 25 nm respectively). These nanowires, well separated with sharp edges, thus project a large surface area. The additional growth on these pine trees like features is shown in detail in Figure 2(e). The figure shows two kinds of structures: coagulated nanowires which appear as a hierarchical aggregate and a flower like structure of size around 2 to 4 μm. A magnified view of micron sized flower is presented in Figure 2(f) which shows a four to six lobed structure with a central depression filled with vertical structures of length 1 to 2 μm and width less than 40nm. A high resolution image of the centre of microflower region is shown in Figure 2(g). The figure shows that besides the long wires, there are also 5 nm wide and 100 nm long sheets present in this region. These nanowires and nanosheet or nanowalls of iron oxide offer high surface area and may have wide applications in field emitters and sensors[9], [19-20].

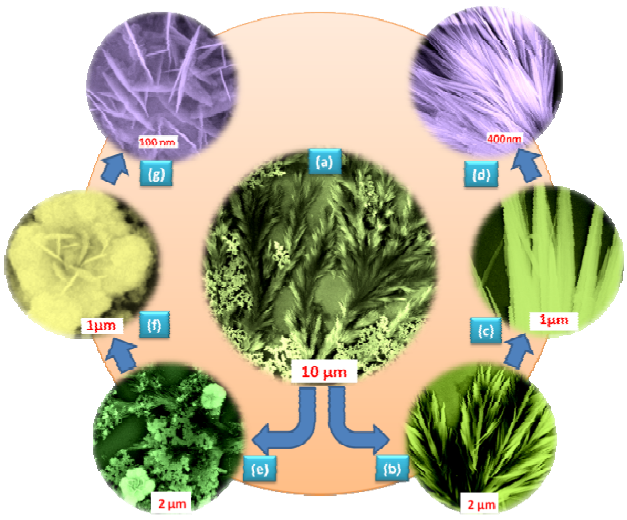


Figure 2. is an FESEM images of (a) film grown for 72 hours, (b) pine shaped structure, (c) an apex of branches of pine shaped structure, (d) the nanorods bundles of branch observed of pine shaped feature, (e) dense overgrowth over pine shaped structure, (f) mico flower, and (g) nanowalls bundles observed at the centre of microflower.

The XRD patterns of films grown for 6 and 72 hours are shown in Figure 3. Both the XRD patterns are corrected with respect to high intensity reflection peak of Si(001) observed at 2Θ=69.7° (JCPDS card No. 80-0018; the position of peak corresponding to 400 reflection of FCC Si(001) is not shown in the figure). The characteristic peaks for α-$Fe_2O_3$ occur at 2Θ=24.2°, 33.2°, 35.7°, 49.6°, 54.2°, and 62.6° corresponds to (012), (104), (110), (024), (116), and (214) reflections (JCPDS card No. 89-8103). The characteristic peaks for γ-$Fe_2O_3$ occur at 2Θ=30.3°, 35.6°, 57.3°, and 62.9° corresponds to (220), (311), (511), (440), and (116) reflections (JCPDS card No. 39-1346). XRD pattern (a) is obtained for a film grown for 6 hours with dendritic morphology. The XRD peaks at 2Θ=33.2° and 62.6°, which corresponds only to (104) and (214) reflections for α-$Fe_2O_3$, suggest that the dendritic structure belong to hematite phase of $Fe_2O_3$ (α- $Fe_2O_3$), and is highly crystalline. The pattern (b) shows XRD spectra for a film grown for 72 hours. A broad peak around 2Θ=33.8° with FWHM=2.6°, shown more clearly in the inset, indicates the presence of nanostructures of iron oxide. The broad peak can be deconvoluted into two peaks at 2Θ=33.2° and 35.6°. The peak at 2Θ=33.2° corresponds to (104) reflection of hematite phase of $Fe_2O_3$ (α- $Fe_2O_3$) and the peak at 2Θ=35.6° corresponds to either (110) reflection of α- $Fe_2O_3$ or (311) reflection of γ- $Fe_2O_3$. The presence of another narrower and intense peak at 2Θ=62.6° for the same pattern corresponds to either (214) reflection of α- $Fe_2O_3$ or (440) reflection of γ- $Fe_2O_3$. The broadening of peak in the case of pattern (b) can therefore be

attributed to the presence of both α- and γ- phase of $Fe_2O_3$. Clearly, there is ambiguity in assigning α- and γ- phases of $Fe_2O_3$ on the basis of XRD measurements due to either the overlap of peaks or the proximity (such as 0.4° difference between (110) and (311)) of reflections of α- $Fe_2O_3$ and γ- $Fe_2O_3$) of peaks in various reflections. The absence of peaks related to wuestite FeO (2Θ=35.9°(111), 41.7°(200), 60.5°(220); JCPDS card No. 89-0687) and magnetite $Fe_3O_4$ (2Θ=29.7°(220) and 35.0°(311); JCPDS card No. 89-0951) however suggests that the structures formed in the present work consist of iron in $Fe^{3+}$ valence state only.

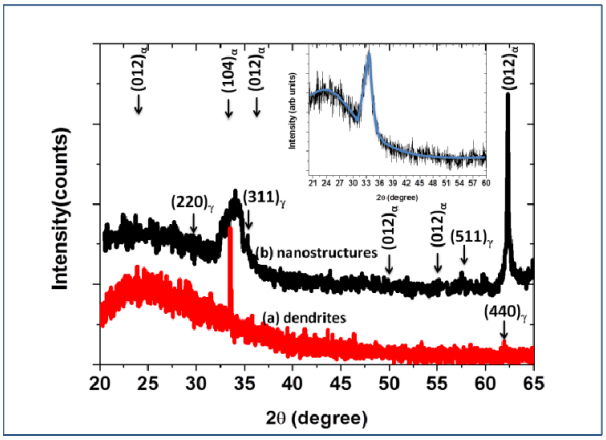


Figure 3. PXRD patterns of film grown for (a) 6 hours with dendritic microstructures, (b) 72 hours with nanostructures and inset shows magnified view of broad peak observed at 2Θ=33.8°.

The ambiguous presence of α and γ phases can be probed by carefully examining the core-level X-ray photoelectron spectra of iron. The spectra obtained for wide-survey scan range of 0–1000eV for films aged to 6 and 72 hours reveal the predominant presence of Fe, O and C from the film surface and Si from the silicon wafer used to support the film. The absence of other elements suggests that there are no by-products or unreacted precursors in the film. The position of core-level spectra of Fe 2p are corrected for the sample charging effect by using C 1s signal at 284.6 eV as reference. The spectra are presented without smoothening. The raw data of Fe 2p spectra (shown in Figure 4) can be decomposed into three contributions corresponding to $2p_{3/2}$ and $2p_{1/2}$ and satellite of $2p_{3/2}$. The Fe 2p core level spectra of film grown up to 6 hours (a) has peaks around 710.8, 718.8, and 724.3 eV correspond to Fe $2p_{3/2}$, shake-up satellite line of $Fe^{3+}$ and Fe $2p_{1/2}$, respectively. In case of film grown upto 72 hours (b) peaks around 711.3, 719.1, and 724.9 eV correspond to Fe $2p_{3/2}$, shake-up satellite line of $Fe^{3+}$ and Fe $2p_{1/2}$, respectively. The peaks corresponding to zero valent Fe ($2p_{3/2}$ at 707 eV), $Fe^{2+}$ ($2p_{3/2}$ at 708 eV) and $Fe^{4+}$ ($2p_{3/2}$ at 713 eV) 24 are not observed which reconfirms XRD observations. The peak around 711 eV corresponds to α- $Fe_2O_3$ and if observed at a lower binding energy of 710.5 eV corresponds to γ- $Fe_2O_3$ [27-35]. The position of typical shake-up satellite peak of $Fe^{3+}$ species in both α and γ $Fe_2O_3$ is expected to be around 8eV higher than the peak for Fe $2p_{3/2}$ maxima[28-35]. On deconvoluting Fe2p photoelectron peak (not shown here), four peaks can be fitted into the spectra: one at 710.8 eV (FWHM=5.0eV) corresponding to $Fe^{3+}(2p_{3/2})$, another at 724.3 eV (FWHM=4.0 eV) corresponding to $Fe^{3+}$ ($2p_{1/2}$), and two others at higher binding energies of 718.8 eV (FWHM=9.0 eV) and 729.3 eV (FWHM=9.0eV) as satellite peaks of $2p_{3/2}$ and $2p_{1/2}$, respectively. The peak at 710.8 eV is assigned to $Fe^{3+}$ ($2p_{3/2}$) state corresponding to α phases of $Fe_2O_3$ [22]. The FWHM of Fe $2p_{3/2}$ peak for 6 hours film is broader than that obtained for 72 hours (shown later) and cannot accommodate another peak. The XPS and XRD measurements thus confirm that the film grown for 6 hours consists of pure α- $Fe_2O_3$ dendritic structures.

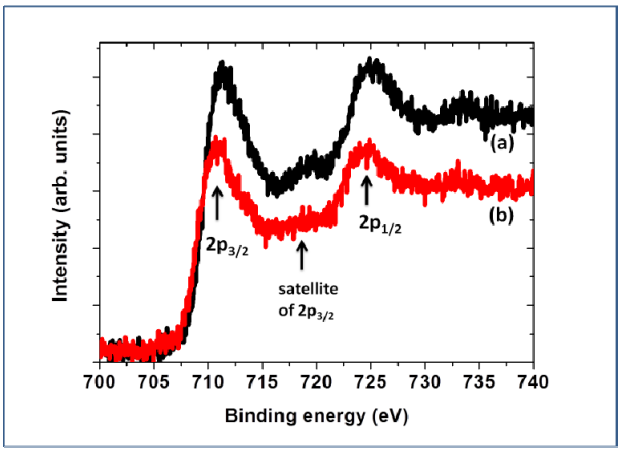


Figure 4. shows core-level Fe 2p XPS spectra of film grown upto (a)6 hours, (b)72 hours.

We now discuss in detail XPS data of Fe 2p corelevel peaks for film grown up to 72 hours. The observed broadening in XRD reflection around 2Θ=33.8° and XPS Fe 2P core-level peak suggest presence of mixed phases of $Fe_2O_3$. We convolute Fe 2p spectrum and subtract Sheryl's background to fit pseudo-voigt function. Figure 5 shows deconvoluted Fe 2p spectra. Figure 5 shows that five peaks can be fit into the spectra: two peaks at 710.2 eV, 711.2 eV corresponding to $Fe^{3+}$ ($2p_{3/2}$), and one peak at 724.3 eV corresponding to $Fe^{3+}$ ($2p_{1/2}$), and two other peaks at higher binding energies of 718.2 and 729.4 eV corresponding to satellite peaks of $2p_{3/2}$ and $2p_{1/2}$, respectively. Area under the $2p_{3/2}$ peak is nearly double of that under $2p_{1/2}$ peak due to spin-orbit (j-j) coupling (degeneracy of states in Fe $2p_{3/2}$ and Fe $2p_{1/2}$ is 4 and 2, respectively). The peak at 710.2 eV (FWHM=4.0eV) can be assigned to $Fe^{3+}$ ($2p_{3/2}$) in α-$Fe_2O_3$ and peak at 711.2 eV (FWHM=2.0eV) can be assigned to $Fe^{3+}$ ($2p_{3/2}$) in γ-$Fe_2O_3$ [22]. The ratio of area under the peaks at 711.2 and 710.2 eV is 5:1 suggests that the amount of α- $Fe_2O_3$ is more than five times the amount of γ- $Fe_2O_3$. Thus both XRD and XPS measurements suggest presence of mixed α- $Fe_2O_3$ and γ- $Fe_2O_3$ films grown up to 72 hours.

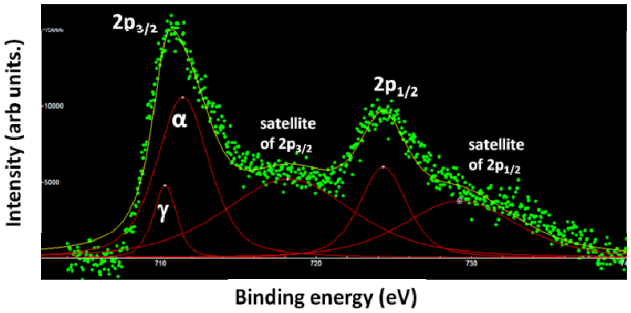


Figure 5. shows deconvoluted spectra of Fe 2p core-level spectra of Iron for a film grown for 72 hours.

On the basis of above discussion, the dendritic microstructure consists of crystalline $Fe_2O_3$. The literature reports suggest that α-$Fe_2O_3$ crystal has higher sticking coefficient for m-plane <1010> than a-plane <11$\bar{2}$0> [35] possibly due to different

barrier for assimilation of $Fe^{3+}$ and $O^{2-}$ ions on the two planes. The α-$Fe_2O_3$ crystal hence prefers to grow faster along <10$\bar{1}$0> direction. The side branches at 30° with respect to the central trunk grow along either <11$\bar{2}$0> or <10$\bar{1}$0> direction[15]. A higher growth rate along m-direction <11$\bar{2}$0> than a-direction <10$\bar{1}$0> leads to higher growth rate of trunk than that of the branches, which eventually determines the observed morphology shown in Figure 6. Fabrication of branched dendritic structures can increase the number of connection points and therefore enhance connectivity and interconnections in these structures.

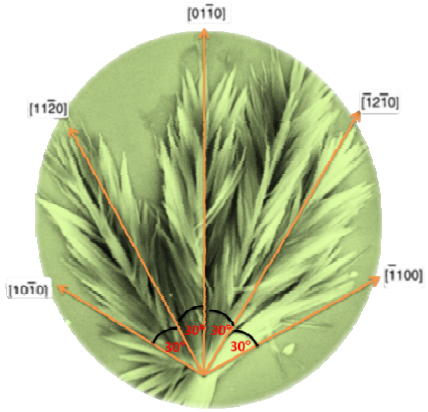


Figure 6. shows leaflets of a pine tree structure shown in Figure 2(b) is superimposed with crystallographic directions of α- $Fe_2O_3$.

The magnetic property of film grown for 72 hours is investigated next. Figure 7 shows the magnetic hysteresis loop recorded at 300K and 10K and the inset shows expanded low field hysteresis loops acquired at (a) 300K and (b) 10K. For higher applied magnetic field of -50K A/m <H< 50K A/m, film grown upto 72 hours shows negligible hysteresis feature with no saturation magnetization at 300K and 10k, suggesting weak ferromagnetic behaviour. At low field, hysteresis at 300K (a) shows saturation magnetisation $M_S$ = 12μ $Am^2/Kg$, coercive field $H_C$ =117 A/m, and remanence $H_R$ =0.44μ $Am^2/Kg$. Hysteresis loop at 10K (b) shows, saturation magnetisation $M_S$ = 60μ $Am^2/Kg$, coercive field of $H_C$ =573 A/m and remanence $H_R$ =7.46μ $Am^2/Kg$. With decrease in temperature from 300K to 10 K, the coercive field and saturation magnetisation increases by nearly five time, but the remanence field increase by 150 times. The observed $M_S$ and Hc values of dendritic γ- $Fe_2O_3$ are very less in comparison to recently reported values (Ms=78.9 $Am^2/Kg$ at 300K and 73.4 $Am^2/Kg$ at 5K, Hc= 320.5 A/m at 300K and 137.5 A/m at 5K )[22]. At 300K, microstructures of α- $Fe_2O_3$ of size 0.1 to 2 μm is reported recently to have Mr value 0.091 to 0.2 $Am^2/Kg$ and Hr value 240 to 1800 A/m [36]. This suggests that the formed dendritic structure in this study may not have γ- $Fe_2O_3$ or may have lesser percentage of γ- $Fe_2O_3$ in the mixed phase of α and γ- $Fe_2O_3$. It is well known that the physical and chemical properties of microstructure or nanostructure depend on size distribution, defect structure and dimensions[15,30]. We infer from XRD, FESEM and XPS study that the $Fe_2O_3$ dendritic structures are highly anisotropic; hence it will be interesting to investigate in future magnetization dependence on structural anisotropy. Since the anisotropy of structures is known to significantly affect saturation magnetisation.

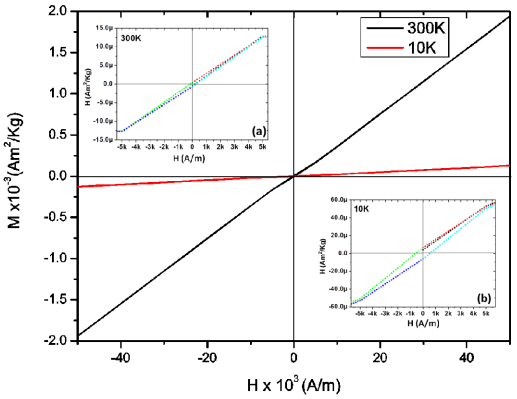


Figure 7. shows magnetic hysteresis loops of film grown for 72 hours at 10K and 300K and low field hysteresis loops at (a) 300K and (b) 10K are shown as inset.

## Conclusions

We have used simple liquid-liquid interface method to form thin film of $Fe_2O_3$. The morphology of nanostructure and microstructure is determined by using FESEM. The crystallinity of the structures is identified by using XRD measurements. The identification of phase of these iron structures is carried out by using XRD and XPS studies. XRD and XPS measurements point to highly crystalline dendritic α- $Fe_2O_3$ at short times which evolve to mixed phase α and γ $Fe_2O_3$ nanostructures at long times (72 hours). The magnetic measurement also indicates the presence of mixed phase in sample grown for 72 hours.

## Acknowledgements

Author thanks IISc, Bangalore, India for a Research Associate Fellowship and IPC and MRC departments of IISc for the measurements

## Notes

* [1]*Department of Chemistry, Lancaster University, Bailrigg, Lancaster, United Kingdom, E-mail:v.srivastava@lancaster.ac.uk*
[2] *Department of Chemical Engineering, Indian Institute of Science, Bangalore, India.*

## REFERENCES

(1) M. Law, D. J. Sirbuly, J. C. Johnson, J. Goldberger, R. J. Saykally and P. Yang. *Science*, 2004, 305,1269.
(2) D. L. Leslie-Pelecky and R. D. Rieke, *Chemistry of Materials,* 1996, 8, 1770.
(3) M. Philip, *Reports on Progress in Physics*, 2001, 64, 297.
(4) J. Irizar, J. Dinglasan, J. B. Goh, A. Khetani, H. Anis, D. Anderson, C. Goh and A. S. Helmy, *Selected Topics in Quantum Electronics, IEEE Journal of,* 2008, 14, 1214.
(5) I. V. Chernyshova, S. Ponnurangam and P. Somasundaran, *Journal of Catalysis*, 2011, 282, 25.
(6) S. Laurent, D. Forge, M. Port, A. Roch, C. Robic, L. Vander Elst and R. N. Muller, *Chemical Reviews*, 2008, 108, 2064.
(7) G. Zhang, S. Sun, M. N. Banis, R. Li, M. Cai, and X. Sun, *Crystal Growth & Design*, 2011, 11, 2493.
(8) Y. Furukawa and W. Shimada, *Journal of Crystal Growth* 1993, 128, 234.

(9) P. Qingtao, H. Kai, N. Shibing, Y. Feng, L. Shumei and H.,Deyan, *Journal of Physics D: Applied Physics*, 2009, 42, 015417.
(10) G.R. Li, C.Z. Yao, X.H. Lu, F.L. Zheng, Z.P. Feng, X.L. Yu, C.Y. Su and Y.X. Tong, *Chemistry of Materials*, 2008, 20, 3306.
(11) J. P. Xiao, Y. Xie, R..Tang, M. Chen and X.B. Tian, *Advanced Materials*, 2001, 13, 1887.
(12) C. Kim, J.G. Oh, Y.T. Kim, H. Kim and H. Lee, *Electrochemistry Communications*, 2010, 12, (11), 1596-1599.
(13) Z. Liu and X. Kong, *Physical Chemistry Chemical Physics*, 2010, 12, 9475.
(14) X. Wu, J. Sui, W. Cai and F. Qu. *Materials Chemistry and Physics*, 2008, 112, 325.
(15) M. Cao, T. Liu, S. Gao, G. Sun, X. Wu, C. Hu and Z. L., Wang, *Angewandte Chemie International Edition*, 2005, 44, 4197.
(16) J. Gu, S. Li, E. Wang, Q. Li, G. Sun, R. Xu and H. Zhang, *Journal of Solid State Chemistry*, 2009, 182, 1265.
(17) Y. Y. Xu, X. F. Rui, Y. Y. Fu and H. Zhang, *Chemical Physics Letters,* 2005, 410, 36.
(18) A. Kay, I. Cesar and M., Grätzel, *Journal of the American Chemical Society*, 2006, 128, 15714.
(19) C. Wu, P. Yin, X. Zhu, C. O. Yang and Y. Xie, *The Journal of Physical Chemistry B*, 2006, 110, 17806.
(20) S. Zeng, K. Tang, T. Li, Z. Liang, D. Wang, Y. Wang, Y. Qi and W. Zhou, *The Journal of Physical Chemistry C*, 2008, 112, 4836.
(21) A. J. Cowan, C. J. Barnett, S. R. Pendlebury, M. Barroso, K. Sivula, M. Grätzel, J. R. Durrant and D. R.,Klug, *Journal of the American Chemical Society*, 2011, 133, 10134.
(22) G. Sun, B. Dong, M. Cao, B. Wei, C. Hu, *Chemistry of Materials,* 2011, 23,1587.
(23) T. J. Daou, J.M. Greneche, S.J. Lee, S. Lee, C. Lefevre, S. Begin-Colin and G. V. Pourroy, *The Journal of Physical Chemistry C* 2010, 114, 8794.
(24) D. Yogev and S. Efrima, The Journal of Physical Chemistry, 1988, 92,5754.
(25) U. K. Gautam, M. Ghosh and C.N.R. Rao, Langmuir, 2004, 20, 10775.
(26) C. D. Wanger, W. M. Riggs, L. E., J. F. DavisMoulder and G. E. Muilenberg, *Handbook of X-ray Photoelectron Spectroscopy*, Perkin-Elmer Corp., Physical Electronics Division, Eden Prairie, Minnesota, USA, 1979. PP.190.
(27) T. Yamashita and P. Hayes, *Journal of Electron Spectroscopy and Related Phenomena*, 2006, 152, (1–2), 6-11.
(28) T. Yamashita and P. Hayes, *Applied Surface Science*, 2008, 254, 2441.
(29) C.J. Jia, L.D. Sun, F. Luo, X.D. Han, L. J. Heyderman, Z.G. Yan, C.H. Yan, K. Zheng, Z. Zhang, M. Takano, N. Hayashi, M. Eltschka, M. Kläui, U. Rüdiger, T. Kasama, L. Cervera-Gontard, R. E. Dunin-Borkowski, G. Tzvetkov and J. R. Raabe, *Journal of the American Chemical Society*, 2008, 130,16968.
(30) T. Fujii, F. M. F. de Groot, G. A. Sawatzky, F. C. Voogt, T. Hibma and K. Okada, *Physical Review B*, 1999, 59, 3195.
(31) D. Zhang, X. Zhang, X. Ni, J. Song and H. Zheng, *Crystal Growth & Design*, 2007, 7, 2117.
(32) C. R. Brundle, T. J. Chuang and K. Wandelt, *Surface Science,* 1977, 68, 459.
(33) P. C. J. Graat and M. A. J. Somers, *Applied Surface Science 1996*, 100–101, 36-40.
(34) P. Mills and J. L., Sullivan, *Journal of Physics D: Applied Physics,* 1983, 16, 723.
(35) S. Thevuthasan, Y. J. Kim, S. I. Yi, S. A. Chambers, J. Morais, R. Denecke, C. S. Fadley, P. Liu, T. Kendelewicz and G. E. Brown Jr, *Surface Science* 1999, 425, 276.
(36) J. Sun, K. L. Wu, X. Z Li, C. Dong, X.W. Wei, X.W. Wang, B. Zhang, Z. X. Zhang and J. R. Huang Cryst Eng Comm 2014,16, 6873-81